Investigation of the opacity binning approach for solving the shock-generated radiation of the Apollo AS-501 re-entry

By A. A. Wray†, J.-F. Ripoll‡ AND D. Prabhu¶

We investigate the Opacity Distribution Function (ODF) approach by solving for the radiation in a simulated Apollo AS-501 re-entry. The ODF method groups the photons into bins of similar opacity and is compared to the usual multi-group method in which the photons are simply grouped according to frequency. We show that the ODF method gives an accurate solution of the re-entry problem when discretizing the RTE into 10 opacity bins, as compared to using the full set of $\sim 10^7$ frequencies. We show that the same order of accuracy is obtained by the multi-group method if $10,000$ frequency groups are used. The ODF method thus allows a huge reduction in numerical cost in the RTE solution and is found to be effective for radiation in hypersonic re-entry.

1. Motivations and objectives

For calculating radiation in re-entry problems, the variation of the radiation with frequency must be addressed. Complex frequency dependence appears in both the source function and the opacity field of the radiative transfer equation (RTE). This complexity is due to a very large number of bound-bound and bound-free transitions happening in very hot, partially ionized, non-equilibrium air. Full resolution of the problem is possible but requires treatment of the radiation transport at $\sim 10^7$ frequencies. Such computations are commonly done at NASA/Ames using the NEQAIR96 code (Whiting *et al.* 1996) to post-process flow field data. This fully-resolved approach is infeasible in a time-dependent computation due to extreme computational cost. There exist many methods to reduce the cost of the solution, and we can divide these into two families (Mihalas & Mihalas 1999). One can divide the frequency spectrum into n_g contiguous groups, average, and solve the transport for each group; these are the multi-group methods. Or one can re-organize the frequency spectra into n_b opacity "bins" or "pickets" according to the value of the opacity (Mihalas & Mihalas 1999). This creates disjoint sets of ν's, the bins or pickets, with similar mean opacities. The second method is usually referenced as the Opacity Distribution Function (ODF) method and as been in use for many years (Strom & Kurucz 1966; Mihalas & Mihalas 1999; Kurucz 1970; Kurucz 1979; Nordlund 1982; Mihalas & Auer 2001). It is based on the key *recognition that transport depends on the value of the opacity not the value of the frequency*, as stated in Auer and Lowrie (2000). In its usual and sophisticated form, the ODF method, also called the multi-band method (Cullen & Pomraning 1980), merges both approaches by reorganizing the opacity into n_b bins inside each of n_g groups. Many other methods for rearranging the frequencies or the opacities exist for reducing the cost of the RTE; these are reviewed in Modest (2003).

† NASA Ames Research Center
‡ Los Alamos National Laboratory, ISR-2
¶ ELORET Corporation

We will compare here the results of (1) the multi-band technique in which $n_g = n$ groups are defined but with a single bin $n_b = 1$ inside each group (this is simply the multi-group approach), versus (2) the multi-band technique where a single group is defined for the whole spectrum ($n_g = 1$) but which is divided into $n_b = n$ bins. For simplicity and clarity we will designate this as the multi-bin method. The multi-bin method has notably been used by astrophysicists for solar computations (Nordlund 1982; Stein & Nordlund 2000; Vogler *et al.* 2004). The goal of this paper is to compare the multi-group and multi-bin methods for the Apollo AS-501 re-entry. We will demonstrate that the method allows solution of this re-entry radiation problem with high accuracy for a very low number of bins (10 bins), an accuracy that is not attained by the multi-group approach even with a much larger number of groups.

2. The binning algorithm and equations

To define our notation, we write the time-independent radiative transfer equation for direction $\mathbf{\Omega}$, source $S(\nu, \mathbf{x})$, opacity $\sigma(\nu, \mathbf{x})$, and intensity $I(\nu, \mathbf{x})$ as follows:

$$\mathbf{\Omega} \cdot \nabla_{\mathbf{x}} I(\nu, \mathbf{x}) = \sigma(\nu, \mathbf{x})(S(\nu, \mathbf{x}) - I(\nu, \mathbf{x})). \tag{2.1}$$

We have suppressed the dependence of I on $\mathbf{\Omega}$ for simplicity of notation. We also use simply $\mathbf{x}$ to denote all spatial coordinates.

In order to create the bins in ν-space, we first define an $\mathbf{x}$-independent mean opacity, $\langle\sigma\rangle(\nu)$, which is formed by weighting with the source as follows:

$$\langle\sigma\rangle(\nu) = \frac{\int_{\mathbf{x}} S(\nu, \mathbf{x})\sigma(\nu, \mathbf{x})dx^3}{\int_{\mathbf{x}} S(\nu, \mathbf{x})dx^3}. \tag{2.2}$$

The bins are defined using a mean opacity so as to be the same for all spatial points. The set of frequencies in bin i is defined to be

$$\{\nu_i\} = \{\nu \mid \langle\sigma\rangle(\nu) \in [\sigma_{i-\frac{1}{2}}, \sigma_{i+\frac{1}{2}})\}. \tag{2.3}$$

The dividing values $\sigma_{i-\frac{1}{2}}, \sigma_{i+\frac{1}{2}}$ are chosen to be equally spaced logarithmically, i.e., $\sigma_{i-\frac{1}{2}}/\sigma_{i+\frac{1}{2}} = \text{const.}$ for all i.

Next we integrate the RTE Eq. (2.1) over each bin i. This leads to an unclosed term

$$\int_{b(\nu)=i} \sigma(\nu, \mathbf{x})I(\nu, \mathbf{x})d\nu, \tag{2.4}$$

where we have written $b(\nu) = i$ if frequency ν is in bin i, i.e., if $\langle\sigma\rangle(\nu) \in [\sigma_{i-\frac{1}{2}}, \sigma_{i+\frac{1}{2}})$. We approximate Eq. (2.4) by defining a mean opacity over the ith bin, $\bar{\sigma}_i(\mathbf{x})$, in a source-weighted manner:

$$\bar{\sigma}_i(\mathbf{x}) = \frac{\int_{b(\nu)=i} S(\nu, \mathbf{x})\sigma(\nu, \mathbf{x})d\nu}{\int_{b(\nu)=i} S(\nu, \mathbf{x})d\nu}. \tag{2.5}$$

If the source $S(\nu, \mathbf{x})$ were Planckian, which it is not in the Apollo case, Eq. (2.5) would be the Planck mean opacity in a bin (Mihalas & Mihalas 1999). The unclosed term is approximated as

$$\int_{b(\nu)=i} \sigma(\nu, \mathbf{x})I(\nu, \mathbf{x})d\nu \approx \bar{\sigma}_i(\mathbf{x}) \int_{b(\nu)=i} I(\nu, \mathbf{x})d\nu. \tag{2.6}$$

Mean opacities other than Eq. (2.2) and Eq. (2.5) could of course be used to define

the bins and to approximate the unclosed term in the bin-integrated RTE. Complex means as those of Patch (1967) and Ripoll *et al.* (2001) could, for instance, be used. Two obvious possibilities are the simple arithmetic (unweighted) and the Rosseland means. We have experimented with these two means using artificially generated source and opacity functions and, for the unweighted mean opacity, using the Apollo data as well. In nearly all instances the source-weighted form gives more accurate results, though there are some cases in which the unweighted form is slightly more accurate, but this is outweighed by other instances in which this mean is much less accurate than the source-weighted one.

The total source function in bin i, S_i, is simply

$$S_i(\mathbf{x}) = \int_{b(\nu)=i} S(\nu, \mathbf{x}) d\nu. \tag{2.7}$$

We can now write the RTE for each bin i as

$$\mathbf{\Omega} \cdot \nabla_{\mathbf{x}} I_i(\mathbf{x}) = \bar{\sigma}_i(\mathbf{x})(S_i(\mathbf{x}) - I_i(\mathbf{x})), \tag{2.8}$$

where I_i is the total intensity in bin i: $\int_{b(\nu)=i} I(\nu, \mathbf{x}) d\nu$. The only approximation is Eq. (2.6). Because the binning is not $\mathbf{x}$-dependent, the spatial derivative operator commutes with the binning operation.

The final step is to discretize ν-space. For the Apollo data, the already-discretized set of frequencies $\{\nu_j\}$ is simply divided into bins using Eq. (2.3) to form a subset $\{\nu_{i_k}\}$ for each bin i:

$$\{\nu_{i_k},\, k = 1...k_{\max}\} = \{\nu_j \mid \langle\sigma\rangle(\nu_j) \in [\sigma_{i-\frac{1}{2}}, \sigma_{i+\frac{1}{2}})\}. \tag{2.9}$$

In general, the number of frequency samples per bin, $k_{\max}$, will vary from bin to bin.

In the multi-group case, the same steps are followed, but the quantities are integrated over contiguous ν-subsets of equal size; that is, the grouping method chosen is simply to divide all of ν-space into equal-sized groups. We recognize that this might not be an optimal choice of groups.

3. The Apollo AS-501 re-entry data

The AS-501 flight was chosen because its flight trajectory was, by design, very similar to those of spacecraft returning from the moon and hence generated the highly non-equilibrium shock layer that will be present in future Crew Exploration Vehicle (CEV) re-entries from the moon and Mars.

The radiation field of the Apollo AS-501 re-entry has been simulated using data from the NEQAIR96 code (Whiting *et al.* 1996). NEQAIR has been largely used at NASA/Ames and is, for instance, well described and referenced in Moreau (1993).
NEQAIR96 was used to generate the source and opacity as functions of space for 1.09×10^7 frequencies and also to compute the radiative intensity along a line leading from the shock layer to the stagnation point of the vehicle. The source and opacity were calculated from the following hydrodynamic quantities: kinetic temperature, electron temperature, rotational and vibrational temperatures, and species concentrations of the non-equilibrium air plasma. Such a detailed hydrodynamic data set cannot be obtained from measurements since it requires a large number of physical quantities at high spatial and temporal resolution. The hydrodynamic quantities needed by NEQAIR96 were obtained from simulations with the DPLR code (Wright *et al.* 1998) of NASA/Ames and validated against existing measurements.

In Fig. 1, we plot the source function at the shock (left) and at the nose of the vehicle

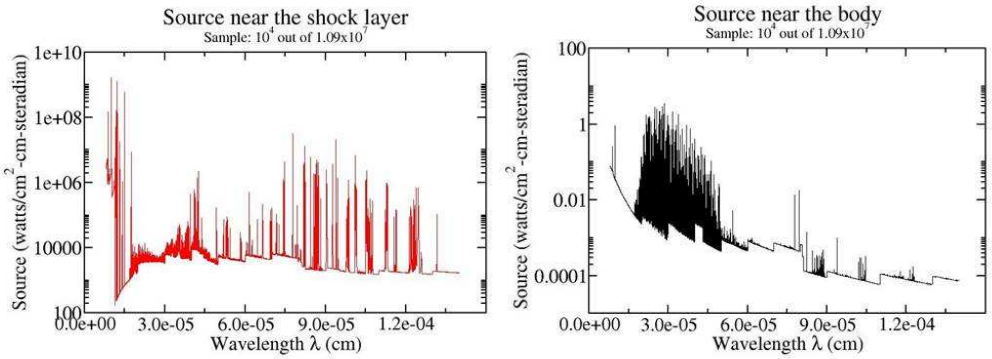

FIGURE 1. Sample of the source $S(\nu)$ near the shock (left) and near the body of the vehicle (right). One out of every 10^4 wavelengths is shown.

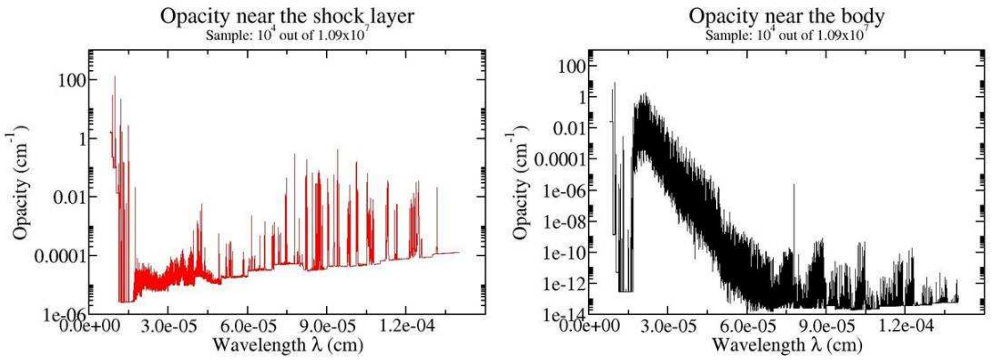

FIGURE 2. Sample of the opacity $\sigma(\nu)$ near the shock (left) and near the body of the vehicle (right). One out of every 10^4 wavelengths is shown.

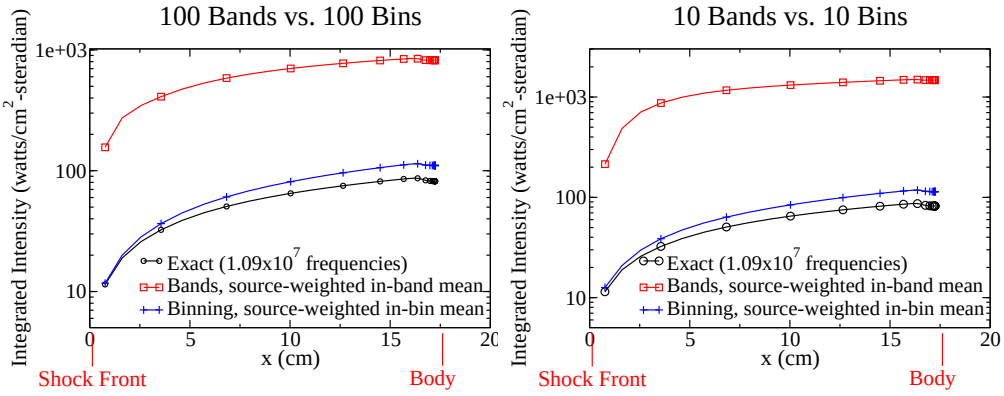

FIGURE 3. Comparison of the radiative intensity (W/cm^2-steradian) computed with $n_g = n_b = 100$ (left) and with $n_g = n_b = 10$ (right).

(right). Similarly, the opacity is shown in Fig. 2. Both profiles attest to the complexity of the problem.

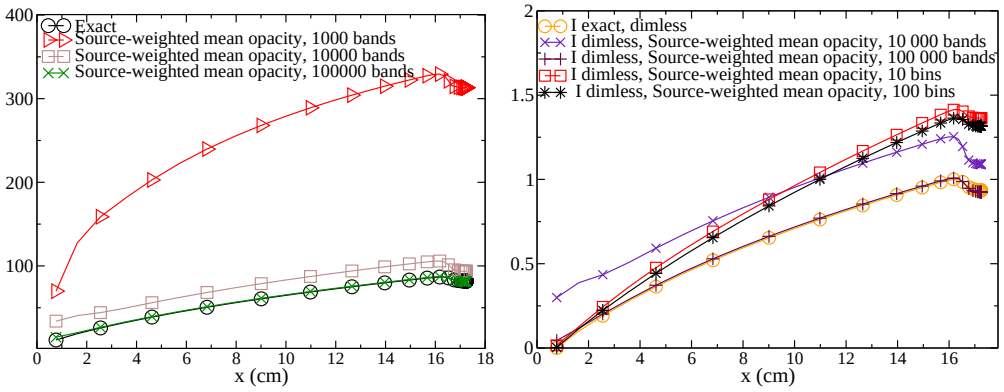

FIGURE 4. Comparison of the radiative intensity (W/cm^2-steradian) computed with 1 000, 10 000 and 100 000 groups (left). Dimensionless intensities compared for different bin and group numbers (right).

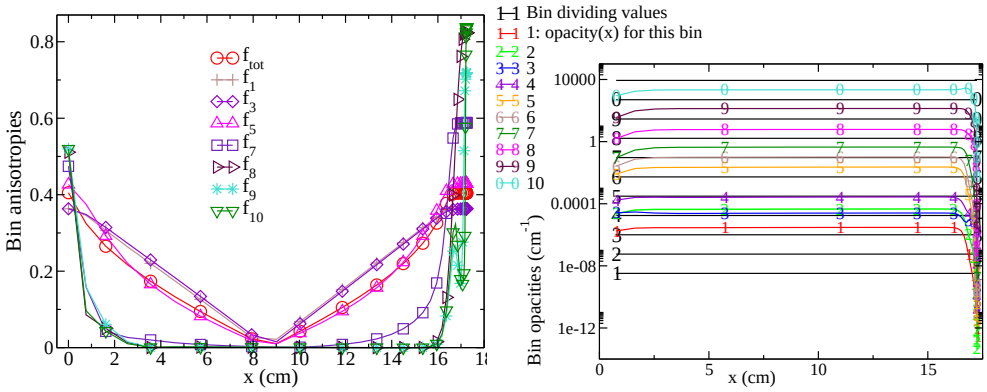

FIGURE 5. Total and bin anisotropies (left) and source weighted opacities and bin opacity boundaries (right), where the 10^{th} bin is denoted 0.

4. Numerical results

We first compare two computations of the radiative intensity, one with 100 frequency groups and one with 100 bins ($n_g = n_b = 100$). The results are shown in Fig. 3 (left) along with the exact solution, i.e., the intensity computed as the sum over all 1.09×10^7 frequencies of the dataset, each separately transported. The solution obtained with 100 bins is very close to the exact solution whereas the multi-group solution is off by factors up to 15. Two coarser computations have been done using 10 groups and 10 bins, and these results are compared with the exact solution in Fig. 3 (right). The multi-group solution is off by factors of 10 to 20, and little improvement occurs in going from 10 groups to 100. This implies that a much larger number of groups is likely to be needed to reach good accuracy, a conclusion verified below. On the other hand, the 10-bins solution is already very close to the exact one and to the solution obtained with 100 bins. This confirms that only a few bins are needed to capture an accurate profile, as Auer and Lowrie (2000), Stein and Nordlund (2000), and Vogler *et al.* (2004) have noted in other contexts. It also shows that the convergence process is very fast to a fairly accurate solution. However, increasing the number of bins to 1 000 does not result in substantial improvement. This is presumably due to a strong frequency dependence of the source

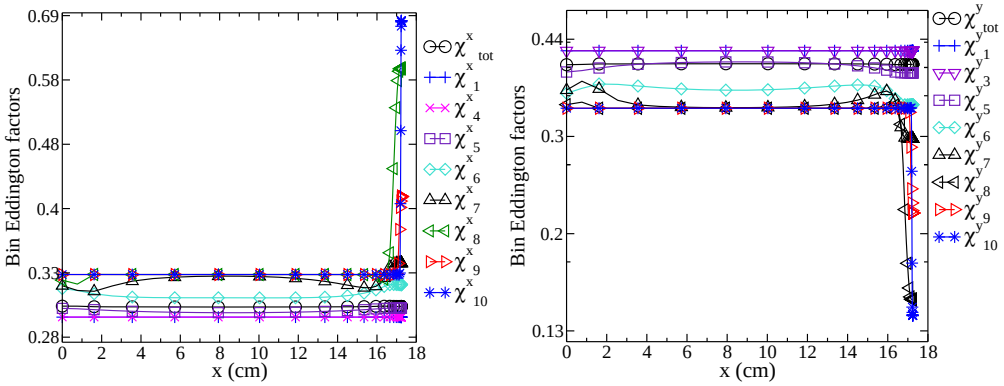

FIGURE 6. Total and bin Eddington factors; xx-component (left) and yy-component (right) computed with 10 bins.

and opacity within a bin at points where the radiation is far from equilibrium. Such a situation causes the approximation Eq. (2.6) to be of poor accuracy.

We now investigate the question of convergence of the multi-group method. In Fig. 4 (left), it can be seen that the 10 000-band solution reaches an acceptable accuracy, while the 100 000-band solution is almost exact. This confirms that a high number of bands is required for accurate results. In Fig. 4 (right), we plot a dimensionless form of the intensity, $(I - I^{\min}_{\text{exact}})/(I^{\max}_{\text{exact}} - I^{\min}_{\text{exact}})$, and compare this quantity for solutions using a small number of bins/bands to those using a large number. The results show that the 10 000-band method gives accuracy comparable to the 100 bin method and that the 100 000-band method has reached near-equivalence to results using all 1.09×10^7 frequencies. If one can afford a large number of frequency subintervals, bins or bands, $\gg 5\,000$, we recommend the use of the multi-group methods due to their simplicity. However, if one wants to use $\lesssim 100$ frequency subintervals, we recommend the use of the multi-bin methods. In our case, we have demonstrated that the 10-bin solution achieves a reasonable accuracy. We believe that the accuracy of the multi-bin method could be improved if the local opacity was used to define the bins. This would lessen the chance that some spatial points would have high variability with frequency within a bin but leads to non-commutivity between the spatial derivative and the bin integral in the integrated RTE.

We next consider the angular variability of the radiation. In Fig. 5 (left), we plot the anisotropy $f = |\mathbf{F}_{\text{R}}|/(cE_{\text{R}})$ and the Eddington tensor $\mathbf{P}_{\text{R}}/E_{\text{R}}$, where E_{R}, F_{R} and $\mathbf{P}_{\text{R}}$ are the radiative energy, flux, and pressure (Mihalas & Mihalas 1999) for each bin, obtained from the 10-bin computation. For $\mathbf{P}_{\text{R}}$, both the normal-normal component of the pressure tensor, denoted χ^x, and the tangent-tangent component, denoted χ^y, are plotted in Fig. 6. Only 8 angles have been used in the angular quadrature to obtain $\mathbf{F}_{\text{R}}$ and $\mathbf{P}_{\text{R}}$, and a tangent-slab approximation has been used to obtain the angular dependence of the radiation. In this case, we have $\sum_{i=1..3} P^{ii}_{\text{R}} = 1$, $P^{ij}_{\text{R}} = 0$ if $i \neq j$, and $P^{22}_{\text{R}} = P^{33}_{\text{R}}$. This leads to $P^{22}_{\text{R}} = (1 - P^{11}_{\text{R}})/2$, which is equivalent to $\chi^y = (1 - \chi^x)/2$. The lowest bin number has the lowest source-weighted spatial mean opacity, and the highest bin number has the highest. It can be seen that the anisotropy of the low-numbered bins is higher than 0.3, with $f \sim 0.4$ in regions close to the nose and body. For the high-numbered bins, the anisotropies are close to 0, as expected, except at the body where quite high values are found: $0.5 < f < 0.85$. This shows that the opacity in this region must be

substantially lower than the spatial-mean opacity for these bins; this is confirmed in Fig. 5 (right). This can also been seen in the plot of the Eddington tensor in Fig. 6: most values are around 1/3, with some lower and with departure from this equilibrium value close to the body for high-numbered bins. Since the solution accuracy in this region is also reduced, one can conclude that the opacity in some bins is becoming highly variable as a function of ν and low enough for some ν that I differs strongly from S, causing Eq. (2.6) to be a poor approximation. In Fig. 5 (right), we can see that, close to the body, the opacity deviates strongly from the global-mean-based bin values, toward lower values. For bins lower than 5, this should have no impact on the accuracy of the bin solution since the opacity of these bins is already very low ($< 10^{-3}$ cm^{-1}). Similarly, we can also see that the values of the local opacities of those bins deviate by one or two bins from their respective global-mean-based bin values on most of the domain ($0 < x < 16$). But since the 10 bins solution is overall quite accurate in this domain, we conclude that this deviation does not have a strong impact. Again, this is due to the very low opacities of those bins ($< 10^{-3}$ cm^{-1}). However, as could be seen in the previous plots, if the semi-opaque and opaque bins have local transparent opacities, which happens for bin 6 to 10 close to the body, then an important loss of accuracy occurs.

5. Conclusions

We have demonstrated that the radiation problem of the Apollo AS-501 re-entry can be solved accurately by discretizing the RTE into 10 opacity bins, instead of using the full set of $\sim 10^7$ frequencies. This leads to a huge reduction in numerical cost in the RTE solution. In addition, we have shown that it is not possible to obtain such a high accuracy by using a small number of frequency groups. In fact, 10 000 groups are needed to obtain the same order of accuracy as the 10-bin solution. We have thus confirmed that the ODF method is effective for the radiative transfer problem in hypersonic re-entry.

Both the multi-bin and multi-group methods obviously converge to the exact solution as the number of bins/groups approaches the total number of resolved frequency points, with the slight caveat for binning that if two or more frequencies have exactly the same opacity, so that they fall in the same bin no matter how many bins are used, then the individual intensities for those frequencies can never be separately computed. But the point of the current work is to construct a method that allows accurate answers with a very small frequency-space sampling. This is to allow fully coupled radiation-hydrodynamics simulations of re-entry to be affordable on current computers. As just noted, the multi-bin method seems to satisfy this need, though checking with other re-entry datasets must certainly be done. Finally, it should be noted that the computation of the mean opacities Eq. (2.5) and of the bin-total source Eq. (2.7) still form the dominant computational cost.

Acknowledgments

We thank Dr Sephane Moreau for fruitful discussions on NEQAIR96 (Moreau 1993). The second author's work was funded by the Department of Energy / National Nuclear Security Agency.

REFERENCES

Auer, L.H., Lowrie, R.B. 2000 Dispersion analysis of radiation/thermal fronts with fully resolved spectral opacity variation. *Los Alamos report LA-UR-00-6094*.

Cullen, D.E., Pomraning, G.C. 1980 The multiband method in radiative transfer calculations. *JQSRT*, **24**, 97–117.

Kurucz, R.L. 1970 Atlas: a computer program for calculating model stellar atmospheres. *SAO Special Report 308*.

Kurucz, R.L. 1979 Model atmospheres for G, F, A, B, and O stars. *App. J. Supplement*, **40**, 1–340.

Mihalas, D., Auer, L.H. 2001 On laboratory-frame radiation hydrodynamics. *JQSRT*, **71**, 61–97.

Mihalas, D., Mihalas, B. 1999 Foundations of radiation hydrodynamics. Dover.

Modest, M.F. 2003 Radiative heat transfer. 3rd ed., McGraw-Hill.

Moreau, S. 1993 Computation of high altitude hypersonic flow field radiation. *PhD. Thesis*, Stanford University.

Nordlund, A. 1982 Numerical simulations of the solar granulation. I. Basic equations and methods. *A&A*, **102**, 1–10.

Patch, R.W. 1967 Effective absorption coefficients for radiant energy transport in nongrey, nonscattering gases. *JQSRT*, **7**, 611–637.

Ripoll, J.-F., Dubroca, B., Duffa, G. 2001 Modelling radiative mean absorption coefficients. *Comb. Theory Mod.*, **5**, 261–275.

Stein, R.F., Nordlund, A. 2000 Realistic solar convection simulations. *Solar Phys.*, **192**, 91–108.

Strom, S. E., Kurucz, R.L. 1966 A statistical procedure for computing the line-blanketed model stellar atmosphere with applications to the F5 IV star procyon. *JQSRT*, **6**, 59–147.

Vogler, A., Bruls, J., Schussler, M. 2004 Approximations for non-grey radiative transfer in numerical simulations of the solar photosphere. *A&A*, **421**, 741–754.

Whiting, E. E., Park, C., Liu, Y., Arnold, J. O., and Paterson, J. A. 1996 NEQAIR96, Nonequilibrium and Equilibrium Radiative Transport and Spectra Program: Users Manual. *NASA RP-1389*.

Wright, M J, Candler, G, and Bose, D. 1998 Data-Parallel Line Relaxation Method for the Navier-Stokes Equations. *AIAA J.*, **36**, 1603–1609.